Dynamics of Local Isolated Magnetic Flux Tubes in a Fast-rotating Stellar Atmosphere

W. Chou, T. Tajima,

Department of Physics, University of Texas, Austin, TX 78712

R. Matsumoto,

Chiba University, Chiba, Japan, and ASRC, JAERI, Naka, Japan

and

K. Shibata

National Astronomical Observatory of Japan, Mitaka, Japan

Received _____; accepted _____

1. Introduction

The introduction (Vogt and Penrod 1983) and use of the Doppler imaging techniques allow the reconstruction of surface luminosity patterns of rapidly rotating stars. A surprising result provided by these Doppler images was the presence of large, dark starspots appearing at high latitudes. In contrast, sunspots are restricted to a latitude band within 30° of the solar equator and relatively small in size. The Zeeman and magnetic Doppler images suggest that stellar spots are magnetic in nature, just like sunspots (Donati et al. 1992; Saar et al. 1994). One might naturally ask why sunspots are different from some starspots, both in size and distribution. Two possible explanations for the large high latitude starspots have been proposed. One is by Schussler and Solanki (1992): the Coriolis force deflects magnetic flux tube rising through the stellar convection zone towards higher stellar latitudes. The other is by Chou et al. (1997): the magnetic buoyancy of flux tubes at low latitudes is suppressed by the Coriolis force, while flux tubes at high latitudes remain unstable and their longer wavelength perturbations grow faster, forming large active regions. Schussler et al. (1996) made a further analysis on the emergence of flux tubes in stars of $1M_{\odot}$ ranging over different ages and at different rotational speeds. They concluded that the young Sun may have had high latitude spots. However, the shape and distribution of starspots for other types of young stars, which may have magnetic fields and rotational periods different from those of the Sun, remain unknown.

Lower main-sequence stars (spectral types G, K, and M) have deep convection zones. The magnetic activity in these cool stars is believed to be associated with the combination of convection and rotation of the stars (Weiss, 1994) and is similar in essence to, though possibly different in details from, that found in the Sun. It has been known for many years that the Ca II emission is closely correlated with magnetic fields on the Sun. Skumanich et al. (1975) deduced a linear proportionality of Ca^{+} emission to magnetic field strength at

process is determined by the Rossby number. For stars of the same rotational periods P (and hence, the same age), later spectral type stars have deeper convection zones, and thus have larger τ_c and stronger magnetic fields, which may result in higher Ca^+ emission.

Parker (1955, 1966) was the first to propose that magnetic activities observed in the Sun originate from the emergence of magnetic flux embedded in the convection zone. The sunspots are thought to be the foot points of emerging magnetic flux tubes. The physics of emergent flux tubes in the Sun has been discussed in detail in the recent literature using the so-called thin flux tube approximation (see review by Moreno-Insertis 1993; also Caligari et al. 1995; Moreno-Insertis et al. 1994; Fan et al. 1993, 1994; D'Silva & Choudhuri 1993; Wang & Sheeley 1991; Chou & Fisher 1989; Choudhuri 1989; Choudhuri & Gilman 1987). Compared with the current Sun, the young G-type stars, at the age of 3×10^7 years, rotate much faster (100 times faster) and possess much stronger magnetic fields. Young M-type stars have even stronger magnetic fields than young G-type stars. There are evidences showing that stars with strong magnetic fields have large (up to 60% of the surface area) starspots (Byrne 1992). Therefore, the thin flux tube approximation may not apply to these stars and flux tubes with finite dimensions must be considered in order to understand the formation of large spots. To our knowledge, no one has ever carried out of a 'fat' magnetic flux tube appropriate for such a study in three dimensional magnetohydrodynamical (3D MHD) simulation. In what follows we present a linear theoretical analysis and a nolinear MHD simulation of this problem. The advantage of using a fat flux tube is that it has a radius instead of a thread-like ring so that we can study its internal structure, and it more likely corresponds to large spots of stars with strong magnetic fields. In this paper, we study the dynamics of local isolated emergent flux tubes (Matthews et al. 1995), in particular in its nonlinear stage, under the influence of the Coriolis force. We set the tube in a local co-rotating Cartesian frame, and we neglect the magnetic tension force produced by the curvature of the ring, and assume an isothermal background. This work provides

summarize the analyses and the key results. We adopt isothermal hydrostatic equilibrium with a constant gravitational field g in the negative z-direction and a magnetic field of constant β in the $x-$direction. The perturbation is assumed to be in the form

$$\delta\rho = \delta\rho_0(z)\exp(i\omega t - ik_x x - ik_y y). \tag{8}$$

After an appropriate manipulation similar to what have been carried out by Parker (1979), we obtain the linear dispersion relation by the determinant of a 8×8 matrix,

$$\begin{vmatrix}
\frac{i\omega}{4\pi} & 0 & 0 & 0 & -ik_y V_{\rm A}^2 & 0 & 0 & 0 \\
0 & \frac{i\omega}{4\pi} & 0 & 0 & ik_x V_{\rm A}^2 & 0 & 0 & 0 \\
0 & 0 & \frac{i\omega}{4\pi} & 0 & 0 & 0 & ik_x V_{\rm A}^2 & 0 \\
\frac{ik_x}{4\pi} & 0 & \frac{1}{8\pi H} & i\omega & -2\Omega_z & 0 & 2\Omega_y & -ik_x \\
0 & \frac{ik_x}{4\pi} & 0 & 2\Omega_z & i\omega & 0 & -2\Omega_x & -ik_y \\
\frac{1}{4\pi C_{\rm s}^2} & 0 & 0 & 0 & 0 & 1 & \frac{i}{\omega}\frac{(\gamma-1)}{\gamma H} & \frac{-1}{C_{\rm s}^2} \\
0 & 0 & \frac{ik_x}{4\pi} & -2\Omega_y & 2\Omega_x & g & i\omega & \frac{-1}{2H} \\
0 & 0 & 0 & -ik_x & -ik_y & i\omega & \frac{-1}{2H} & 0
\end{vmatrix} = 0, \tag{9}$$

where

$$C_{\rm s}^2 = \frac{\gamma P}{\bar{\rho}}, \tag{10}$$

$$H = \frac{C_{\rm s}^2}{\gamma g}(1 + \frac{1}{\beta}) \tag{11}$$

$$\beta = \frac{8\pi P}{B^2} \tag{12}$$

$$V_{\rm A}^2 = \frac{B_x^2}{4\pi\rho}(= \frac{2}{\beta\gamma}C_{\rm s}^2). \tag{13}$$

From this dispersion relation we find that the magnetic flux instability (or buoyancy) at low latitudes is stabilized when the rotational angular velocity Ω is large enough. The

in the current Sun. The corresponding values for the current Sun and the zero-age G-type star are marked in Fig. 1, and an estimated evolution trace is drawn by a dotted line. The positions of the Sun at its age of 10^8 and 10^9 years characterized by its rotational speeds relative to the current Sun (Rosner and Weiss 1985) are also marked on this trace. Extrapolating from the relation of $\tau_c(B-V)$ in Noyes et al. (1984) to spectral type M stars, assuming that young M stars rotate as fast as young G stars of the same ages, and making another extrapolation to estimate $B(Ro)$, we estimate the strength of magnetic field in a M-type star is one order of magnitude greater than that in a G-type star. Thus the zero-age M-type star has parameters indicated by the dark triangle in Fig. 1 ($\beta \sim 1, \Omega \sim 0.1$), and these are the values we adopt in our simulation. An estimated trace of evolution for a M-type star is drawn by another dotted line assuming that it is parallel to the evolution of a G-type star. We find that M-type stars stay in the unstable region during their evolution , meaning that magnetic fields embedded in a M-type star erupt radially at low latitudes regardless of its age. In contrast, the evolution path of a G-type star crosses the critical Ω_c curve so that a zero-age G-type star (in which low latitudes spots are prohibited) and the Sun have different spots distributions. Caution should be exercised because we have made a rough extrapolation and assumption about the magnetic fields and rotational speed of M-type stars. However, since the M-star evolution curve (the dotted line) is away from the critical Ω_c curve (the thick line) at least one and a half orders smaller in β, the conclusion that M-type stars always stay in the unstable region probably remains valid even if we had underestimated β to one order of magnitude. The dashed line in Fig. 1 corresponds to the relation $B \propto \Omega$ as if the stellar structure (pressure, scale height, etc) were not changed during the evolution. In another word this line corresponds to the quantity $\Omega H/V_A = 0.25$ remaining the same value as the Sun. The physical interpretation is that every point in this line has the same ratio of the Coriolis force to the magnetic buoyancy force.

$z = z_{max} = 8.64H$ so that waves transmit through the top boundary. The simulation starts with a straight cylindrical magnetic flux tube with radius $R = H$. To initiate the dynamics, a small velocity perturbation is added inside the tube,

$$V_x = 0.05 \sin[k_x(x - L)] \cos(k_y y), \tag{17}$$

where the perturbation wavelength $k_x = \frac{2\pi}{L_x/2}$ and $k_y = \frac{2\pi}{L_y}$.

We adopt nearly isothermal value of the adiabatic index $\gamma = 1.05$. In an isothermal atmosphere which is imposed in our simulation to keep the analysis simple, a larger γ has a stabilizing effect of Parker instability. In reality, in the boundary between the convection zone and the radiation zone where we expect magnetic twists are accumulated, the background atmosphere is not isothermal but has temperature gradient slightly below marginal stable for convection. In such a case, we can use a larger γ. The combined effect of the temperature gradient and the Coriolis twisting on buoyant flux tubes will be studied in future works.

3.2. Simulation Results

We show the results from two models: in model 1, the angular velocity $\mathbf{\Omega}$ is in the z-direction, which corresponds to the flux tube sitting at the north pole. In model 2, the x-direction is stellar west and the y-direction is north, and $\mathbf{\Omega}$ lies in the y-z plane having an angle of 45° with the z-axis. This corresponds to the case that a toroidal magnetic flux tube sitting in the latitude of north 45°. We also have a testing model to check our code by setting $\Omega = 0$ and compare the result with the existing studies and have successfully reproduced simulations of magnetic buoyancy in a static inertial frame, similar to the results by Matsumoto et al.(1993)

Figure 2 shows isosurfaces of magnetic field energy density $\|\mathbf{B}\|^2 = 0.5[\rho_0 C_s^2]$. In model

same pattern and are symmetric to each other. However, in Fig. 4, we lose this symmetry. Instead, the field in the preceding spot is slightly greater than that in the following one. We conclude that this east-west asymmetry is due to the presence of the $y-$component of rotational angular velocity Ω_y. This is because the Coriolis force, the cross-product of the rising velocity V_z with Ω_y, is in the negative x-direction. The preceding spot which locates on the right hand side (positive x) of the following one has a lower gas pressure since the plasma has been pushed away towards the following spot. Thus the preceding spot has stronger magnetic field. From Fig. 4 we also note that there is no noticeable poleward (y-direction) motion of the flux tube upon its emerging to the surface.

In order to compare the influence of plasma β on the flux tube dynamics, we set a Model 3 whose configuration is identical to Model 1 except for the plasma β value ($\beta = 10$ for Model 3 and $\beta = 1$ for Model 1). In Fig. 2a (and 2b as well) we note that the flux tube does not deform itself into smaller filaments but rather rises as a whole. Figures 5 (a) (velocity field) and (b) (isocontour of B_x) show the YZ cross section at the center of the flux tube ($x = 10$) for Model 1 at $t = 29.09$. The flux tube expands itself into a mushroom shape as it rises toward a lower density layer. Since the radius of the flux tube is relatively large (one scale height), we conclude that this flux tube should produce large spots on the stellar surface after its buoyancy. Figure 5 (c) shows the isocontour of B_x for Model 3 ($\beta = 10$) at the same cross section as in (a) and (b) at $t = 88.8$. The velocity field for Model 3 is not shown because the buoyant motion has ceased and the velocity becomes small. In contrast to Fig. 5 (b), Fig. 5 (c) shows the flux tube has split into smaller filaments. Tajima and Shibata (1997) pointed out that the general morphology of plasmas with high β tends to be filamentary while that of low β plasmas is cellular or sheet-like. The simulation result shown here agrees with this tendancy: filamentary for high β case (Model 1) and cellular for the low β (Model 1). The value of β in the overshoot region of the current Sun is large ($\beta = 10^5$), hence we can surmise that the thin flux tube simulation applies. However, for

the east-west asymmetry and the tilting of magnetic flux tubes. Another set of authors (Rust & Kumar 1996; Moreno-Insertis & Emone 1996; Matsumoto et al 1996, 1997) studied magnetic flux tubes helically kinked prior to their emergence rise to the surface of the Sun. Ideally one would like to simulate the full evolution of a rising magnetic flux tube with off-axis structures. However, such a real 3D fat flux tube simulation adopting solar parameters is still beyond the current computing power. The simulation shown in this paper is the first one to adopt a real 3D fat flux tube, though it does not adopt solar parameters. Still, it is interesting to make a qualitative comparison of our results with the the solar observation. We compare the latitudinal dependence of the tilt angle and that of the east-west asymmetry in our "fat" tube simulation with those from solar observations. The magnetic helicity, which cannot be studied in thin tube approximation, is also discussed.

Figure 6 shows the tilt angle of the emergent portion of flux tubes as a function of the latitude in both northern and southern hemispheres. The tilt angle is defined as the angle of the thin line in Fig. 3 or Fig. 4 to the latitudinal line (x-direction). Positive values mean that such a thin line is rotated counterclockwise from the horizontal orientation. The tilt angle has a different sign in each hemisphere. In the northern hemisphere, the angle is negative, meaning that a pair of spots are positioned at upper left and lower right; the arrangement is opposite in the southern hemisphere. The absolute value of the tilt angle ranges from zero at the equator, to about 10° at north and south 45° latitude. These results suggest that the correlation of the tilting angle and the latitude of stellar spots in a young M-type star is similar to that in the Sun.

Our simulation results show that the ratio of maximum $|B_z|$ in the preceding foot to that in the following one is slightly greater than unity at low latitudes, ranging from 1.0 to 1.25, indicating that the field strength is just slightly greater in the preceding foot. Two reasons may explain why the ratio is near unity. First, our simulation does not consider the

Pevtsov et al. (1995). It does not help if we reverse the magnetic field in the simulation, because the patterns, the asymmetry, and especially the helicity α remain the same, which follows directly from the basic MHD equations that a sign reversal of B keeps the equation unchanged. This suggests that the helicity observed by Pevtsov et al. (1995) may not be produced by Coriolis twisting of rising-expanding flux tubes, but instead may be the result of the dynamo action with convection column (Kageyama et al. 1995, Yoshizawa & Yokoi 1996). Another possibility is that adopting real solar parameters in the simulation would generate the same helicity results, but it is highly skeptical.

One way to check the accuracy of the code is to compare the linear growth rate with that calculated by linear analysis. Figure 8 shows the time history of $\ln |V_x|$ in Model 1, where V_x is the x-component of velocity at a fixed grid point (chosen at the center of the flux tube). There is a linear growth stage during $7 < t < 15$, and a nonlinear (saturation) stage thereafter. The linear growth rate, which is the slope of the straight line, in our simulation is 0.42. The current existing linear analysis in the literature calculates the growth rate of a 'thin' flux tube (e.g. Spruit & van Ballegooijen 1982, which does not include the effect of rotation, and Ferriz-Mas & Schussler 1994, which includes rotation), an isolated flux sheet (Matsumoto et al. 1993), or continuous field distributions (Chou et al. 1997, and the references cited), but the analysis of a 'fat' flux tube is absent. Comparing the value in our simulation to these linear analysis, we find that the growth rate is identical to that calculated in Matsumoto et al.(1993) and Chou et al.(1997) with wavelength $k_x = 0.6$ and $k_y = 3$ which is adopted as the parameters in our simulation. Therefore, we confirm the accuracy of our MHD code. This growth rate is, however, greater than the value in Spruit & van Ballegooijen (1982). The reason may be that the growth rate of Parker instability is enhanced by interchange modes, but this effect is not included in thin flux tube approximation.

with strong magnetic field (plasma $\beta = 1$) shows this tendency, but it is not significant. Our 3-D fat tube simulation shows the current field from top view. This result is new and can not be obtained by the thin flux tube simulation. We are looking for an observational signature that corresponds to this current field.

The signs of magnetic helicity α obtained in our simulation are opposite in each hemisphere, indicating that the direction of twisting is opposite in each hemisphere. However, these signs are opposite to the existing solar observations. This discrepancy suggests that the observed helicity patterns in the solar surface may not be due to the Coriolis twisting of emerging magnetic flux tubes, and hence other models such as the dynamo action may be needed.

This work was supported by NSF ATM9401128.

Matsumoto, R., Tajima, T., Shibata, K. and Kaisig, M. 1993, ApJ 414,357.

Matsumoto, R., Tajima, T., Chou, W., and Shibata, K. 1996, in Proc IAU Colloquium 153,*Magnetodynamic Phenomena in the Solar Atmosphere-Prototypes of Stellar Magnetic Activity*, ed Uchida, Y., Kosugi, T and Hudson H. S. (Kluwer, Dordrecht) p355.

Matsumoto, R., Tajima, T., Okubo, A., Chou, W., and Shibata, K. 1997, ApJ Letter (submitted).

Moreno-Insertis, F. 1993, in *Solar Magnetic Field*, ed M. Schussler and W. Schmidt (Cambridge University Press, Cambridge) p117.

Moreno-Insertis, F., Caligari, P., and Schussler, M. 1994, Sloar Phys. 153,449.

Moreno-Insertis, F. and Emone, T. 1996, ApJ Letter, 472,153.

Noyes, R.W., Hartmann, S.L., Ducan, D.K., and Vaughan, A.H. 1984, ApJ 279, 763.

Parker, E. N. 1955, ApJ 122,293.

Parker, E. N. 1966, ApJ 145,811.

Parker, E. N. 1979, *Cosmical Magnetic Fields* (Clarendon Press, Oxford) pp 325-331.

Pevtsov, A. A., Canfield, R. C., and Metcalf, T. R. 1995, ApJ Letter 440, 109

Rosner, R. and Weiss, N.O. 1985, Nature 317, 790.

Rust, D. M. and Kumar, A. 1996, ApJ Letter 464, 199.

Sarr, S.H., Piskunov, N.E., and Tuominen, I. 1994, in *Cool Stars, Stellar Systems, and the Sun VIII*, ed Caillault, J.-P., Astro. Soc. Pacific Conf. Ser. Vol. 64, p.661.

Figure Captions

Figure 1 (Solid line) The critical angular velocity Ω_c that stabilized equatorial magnetic flux as a function of the plasma β. It is obtained by the linear analysis and coincidentally identical to $B_{\rm min}$ (see the text for detail) obtained by Schussler and Solanki (1992). The area to the upper-right is the stable region, that is, the buoyancy of flux tubes at low latitudes are largely suppressed by the Coriolis force and hence high latitude spots are expected. The corresponding position for the Sun, young G-type stars at the age of 3×10^7 yr (zero-age G star), 10^8yr, 10^9 yr, and zero-age M-types stars are marked. The dotted lines show possible evolutions of G-type stars and M-type stars. Note that the trace of the evolution line for G-types stars crosses the critical Ω_c curve while the trace for M-type stars stays on the unstable side. The dashed line shows constant $\Omega H/V_A$, which means the ratio of magnetic buoyancy force to the Coriolis force are the same as that in the Sun.

Figure 2 Isosurface of magnetic field energy density $\|\mathbf{B}\|^2 = 0.5[\rho_0 C_s^2]$, for (a) Model 1 (a flux tube at the north pole) at time=29.09 $[H/C_s]$, and (b) Model 2 (a toroidal flux tube at north 45°) at time=28.37 $[H/C_s]$.

Figure 3 The cross section at $z = 4.86$ plane for Model 1 (a tube at the north pole) at time=29.09 $[H/C_s]$, showing (a) the current in the z-direction (J_z), the thin line indicates the tilt angle; (b) the magnetic field in the z-direction (B_z); (c) the current field in this plane; and (d)$\alpha = J_z/B_z$.

Figure 4 The XY-cross section for Model 4 (a toroidal tube at north 45°) at time=28.42 $[H/C_s]$. The meanings of the four figures (a) through (d) are the same as those in Figure 3.

Figure 5 The YZ cross section at $x = 10$ plane (middle of the flux tube) for Model 1

Figure 1

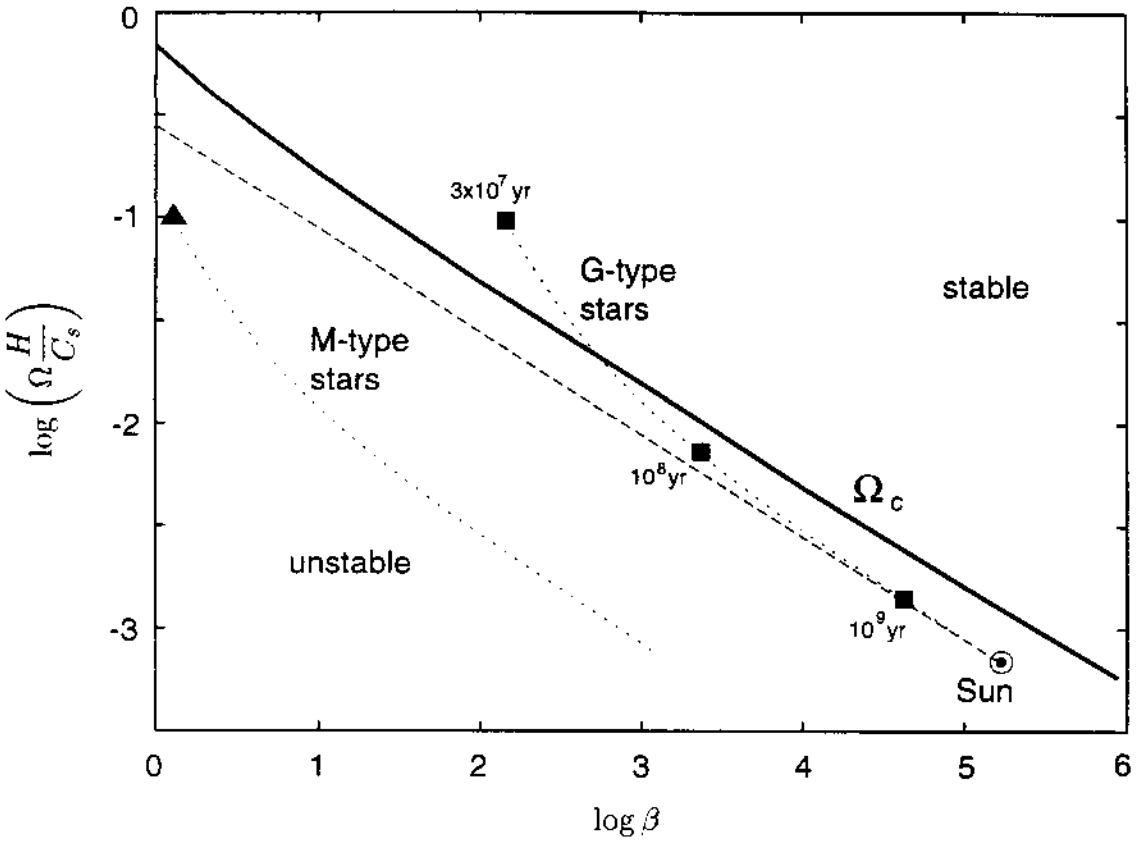
0
-1
-2
-3
0
1
2
3
4
5
6
$\log\left(\Omega\frac{H}{C_s}\right)$
$\log\beta$
3x10^7 yr
10^8yr
10^9yr
G-type
stars
M-type
stars
unstable
stable
Ω_c
Sun

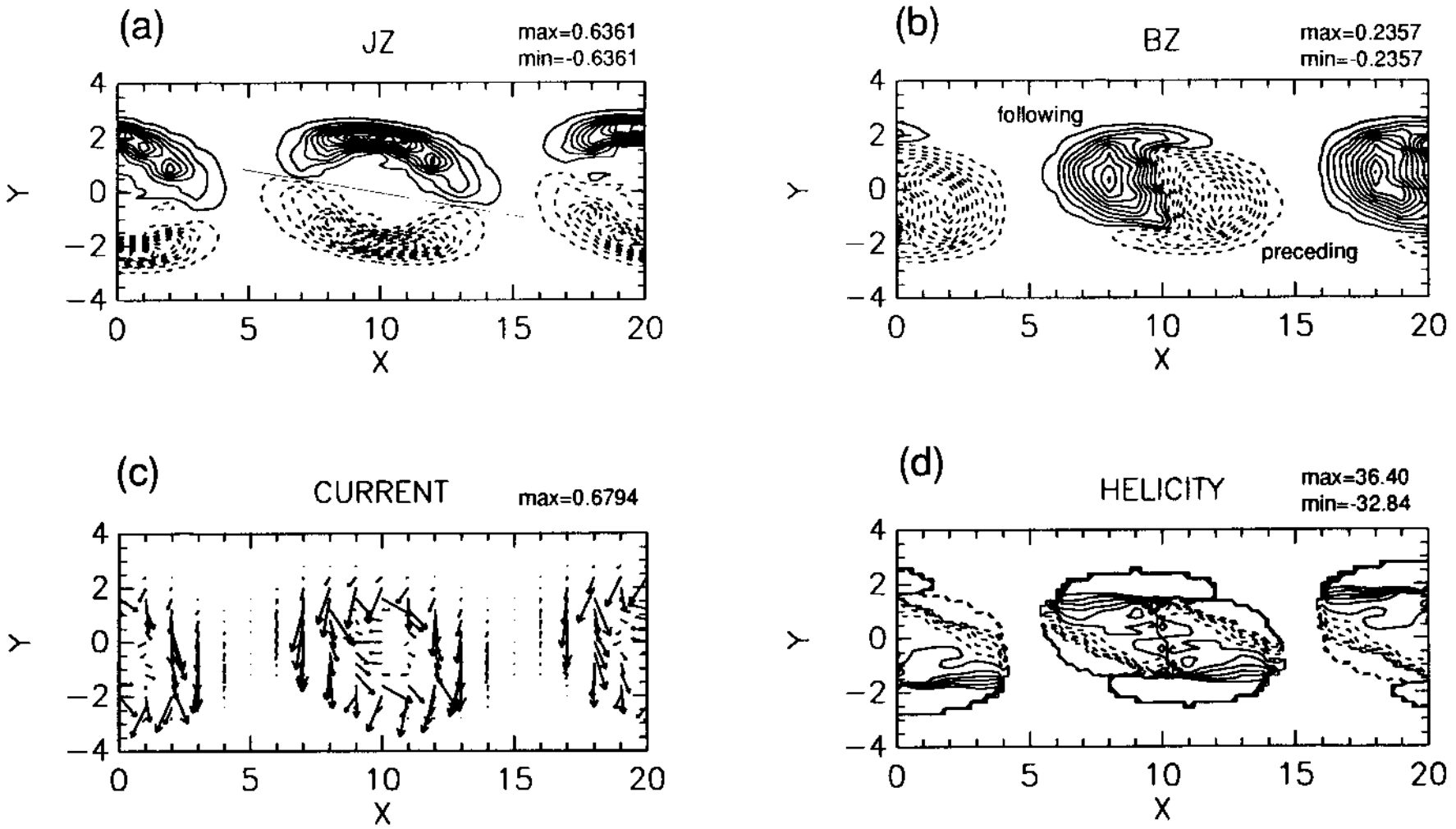
(a)
JZ
max=0.6361
min=-0.6361
(b)
BZ
max=0.2357
min=-0.2357
following
preceding
(c)
CURRENT
max=0.6794
(d)
HELICITY
max=36.40
min=-32.84
X
Y

Figure 3

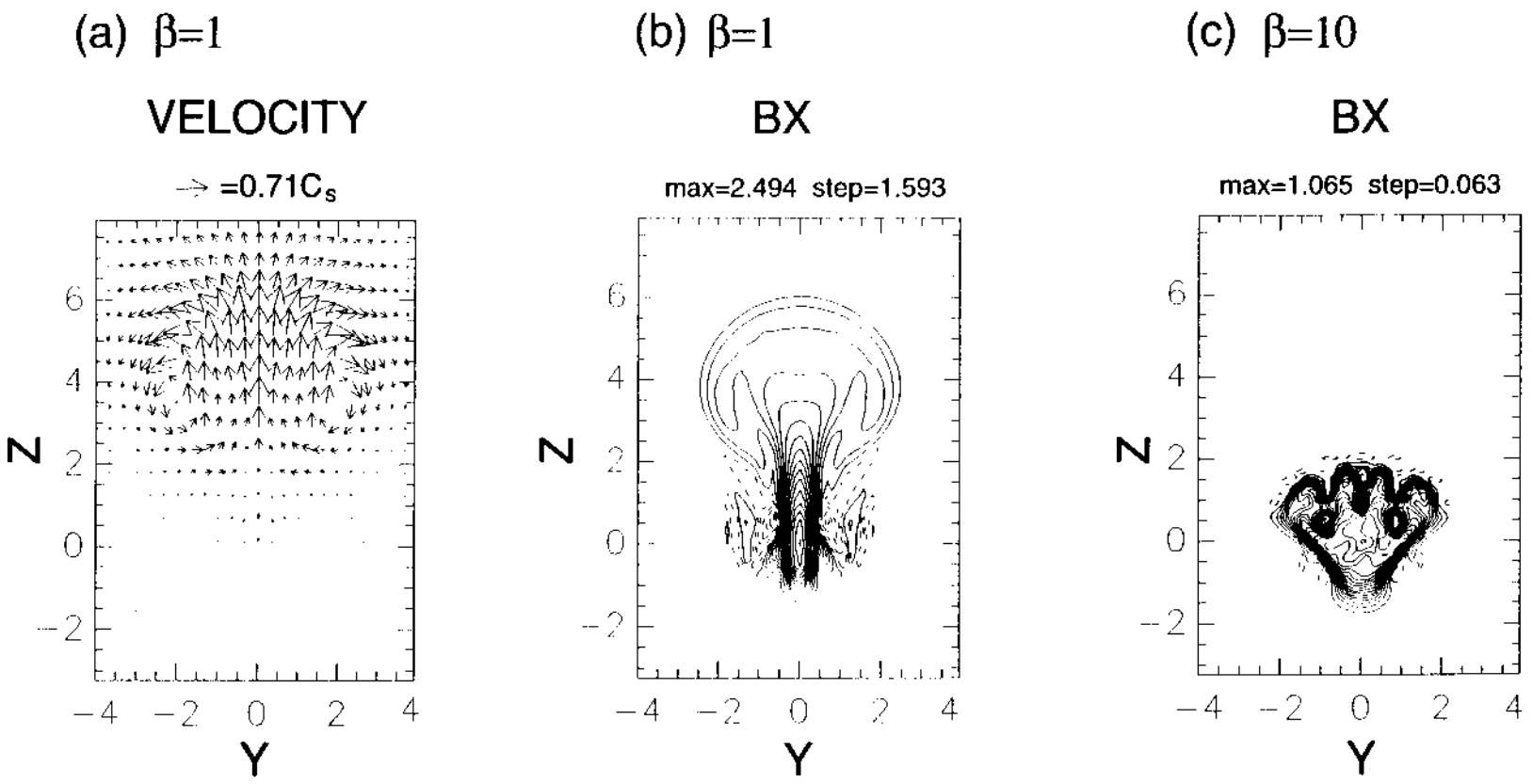
(a) β=1
VELOCITY
→ =0.71Cs
(b) β=1
BX
max=2.494 step=1.593
(c) β=10
BX
max=1.065 step=0.063
Z
Y
6
4
2
0
−2
−4
−2
0
2
4

Figure 5

Figure 8